Optical-Quality Thin Films with Tunable Thickness from Stable Colloidal Suspensions of Lanthanide Oxysulfide Nanoplates

Léna Meyniel, Cédric Boissière, Natacha Krins, Sophie Carenco

Optical-Quality Thin Films with Tunable Thickness from Stable Colloidal Suspensions of Lanthanide Oxysulfide Nanoplates

Léna Meyniel [1], *Cédric Boissière* [1], *Natacha Krins* [1,*], *Sophie Carenco* [1,*]

[1] Sorbonne Université, CNRS, Laboratoire de Chimie de la Matière Condensée de Paris, 4 place Jussieu, 75005 Paris, France

* Corresponding authors e-mail: natacha.krins@sorbonne-universite.fr, sophie.carenco@sorbonne-universite.fr

Abstract: In modern laser technologies, there is a need for coatings that would be compatible with flexible substrates while retaining the advantages of inorganic compounds in terms of robustness. As a first step in this direction, we developed here thin films of lanthanide oxysulfide, of optical quality, prepared by low-temperature dip-coating. As a model compound in the family of oxysulfides, $(Gd,Ce)_2O_2S$ anisotropic nanoplates were used. The films were characterized by scanning electron microscopy (SEM), transmission electron microscopy (TEM), X-ray diffraction (XRD) and *in situ* UV and IR spectroscopic ellipsometry, showing that the bandgap of the materials was preserved through the deposition process. The thickness of the films was tuned in a broad range, from a few nm to 150 nm, using different concentrations of the colloidal suspensions as well as single-layer and multi-layer deposition. Lastly, thermal treatment of the thin films was optimized in order to remove the stabilizing organic ligands of the nanoparticles while preserving their integrity, as confirmed by SEM and XRD.

Keywords: oxysulfide; thin films; dip coating; nanostructured films; cerium; gadolinium; colloids; spectroscopic ellipsometry.

Introduction

Nanostructured thin films have attracted a great deal of interest over the last few decades due to their unique physicochemical features including optical, mechanical and electronic properties. Consequently, they have been exploited as promising devices for a wide range of applications including smart coatings,[1] effective drug delivery systems[2] and highly sensitive sensors.[3] The structuration of thin films from pre-formed colloids is a long-standing challenge considering the deposition variables to be carried out (colloidal stability, particles concentration, withdrawal speed, surface tension, vapor pressure…). Using shaped nanoparticles in colloidal suspension as building blocks provides a mean to trigger self-assembly during deposition.[1,4–6] Moreover, colloidal suspensions of adequate viscosity and surface tension can be used in a well-controlled process such as dip-coating, which offers the opportunity to finely tune the film thickness, a key parameter for further applications. Usual thin films thicknesses vary from a few nm for photocatalysis applications[7] to hundreds of nm for gas and bio sensors.[8,9] Moreover, for deposition on flexible substrates, suspensions of colloidal nanoplates are gaining attention, as they are compatible with a low temperature process.[10–12]

In this research work, we are interested in the design of thin films from a low-temperature deposition process, dip-coating, which may be used for flexible devices, as an example. Laser technologies, and in particular absorption and emission layers, is indeed in demand for such flexible devices.[13] So far, most of them rely on organic layers,[14] easy to process to reach tunable thicknesses,[15] but sometimes subject to photo-bleaching. On the other side, inorganic compounds such as lanthanide oxysulfide phases, of general formula Ln_2O_2S (Ln: lanthanide), present an interest for these technologies,[16] but they were usually deposited by physical deposition such as electron-beam deposition (eg. Y_2O_2S),[17] or only studied as raw micrometric powders (eg. Sm_2O_2S, doped or un-doped).[18,19] Our recent work on lanthanide

oxysulfide nanoplates provides us with a priviledged access to composition-controlled nanoplates with a narrow size distribution, for a large range of Ln. In particular, we mastered the preparation of mixed-lanthanide nanoplates with tunable bandgap and magnetic properties while providing an in-depth understanding of their structural and surface features.[20,21] Although the nanoparticles are covered with oleates at the end of the synthesis, which may hinder their applications based on photoluminescence,[22] we showed that a mild calcination of the powder at 350 °C was enough to remove most of the organic ligands while preserving the crystallographic integrity of the phase.[23] Thus, we propose to explore here the fabrication of thin films of lanthanide oxysulfide with the dip-coating process operated at low temperature. For this study, we selected lanthanide oxysulfide nanoplates of formula $(Gd,Ce)_2O_2S$, which are the best characterized member of the family, presenting in particular a bandgap strongly sensitive to the chemical integrity of the nano-object.

The nanoparticles were prepared following a protocol previously described [20,21] that enabled the formation of small 5 – 10 nm wide and 2 – 3 nm thick nanoplates over the whole $(Gd,Ce)_2O_2S$ composition range with good control of size and crystallinity. The stability of the entire series of the oxysulfide solid solution of $(Gd,Ce)_2O_2S$ nanoparticles was already evaluated with *in situ* X-ray absorption near edge spectroscopy (XANES) and near-ambient pressure X-ray photoemission spectroscopy (NAP-XPS).[21,24] In the doping regime ($Ce \leq 5\%$), cerium plays the dual role of a doping ion and of a nucleus site with its own absorption properties (bandgap). So, for further analysis, the doping regime was restricted to 5% of Ce.

This work presents the design, development and characterization of $Gd_{1.9}Ce_{0.1}O_2S$ nanostructured thin films of optical quality and tunable thickness. The colloidal suspension was optimized in terms of stability to be suited for thin film deposition by dip-coating. Single-layer and multi-layer films were prepared and characterized using SEM-FEG, X-Ray

diffraction and spectroscopic ellipsometry. We were able to deposit fully-formed nanoplates on different substrates as well as control and tune the thickness of the deposition, while keeping the integrity of the nano-sized oxysulfides, as observed through their bandgap and their crystal structure.

Experimental section

Reagents and materials

Oleylamine (OAm; technical grade, 70%), oleic acid (OA; technical grade, 90%), elemental sulfur (S_8; ≥99.5%), sodium oleate (Na(oleate); ≥99%), tetrahydrofuran (THF, ≥99.9%), 2-methyltetrahydrofuran (CH_3THF, >99%), ethanol (CH_3CH_2OH, >96%) and 1-butanol ($CH_3(CH_2)_3OH$, >99%); were purchased from Sigma-Aldrich. 1-octadecene (ODE; technical grade, 90%) was purchased from Acros Organics. Gadolinium acetylacetonate hydrate ($Gd(acac)_3{\cdot}xH_2O$; 99.9%) and cerium acetylacetonate hydrate ($Ce(acac)_3{\cdot}xH_2O$; 99.9%) were purchased from Strem Chemicals. All products were used as received without further purification. 6 inch-diameter p-type (100) Si wafer with a resistivity of 1–10 ohm cm was purchased from Siltronix Silicon Technologies. Fluorine doped-tin oxide thin films on glass substrates were obtained from Solems with a typical coating thickness of 80 nm and a glass thickness of 1.1 mm.

Synthesis of $Gd_{1.9}Ce_{0.1}O_2S$ nanoparticles

The nanoparticles were prepared following a published procedure.[21] In a typical synthesis of $Gd_{1.9}Ce_{0.1}O_2S$, $Gd(acac)_3{\cdot}xH_2O$ (0.475 mmol, 216 mg), $Ce(acac)_3{\cdot}xH_2O$ (0.03 mmol, 10.9 mg), S_8 (0.032 mmol, 8 mg), Na(oleate) (0.50 mmol, 152 mg), OAm (17 mmol, 4.54 g), OA (2.5 mmol, 0.71 g), and ODE (32.5 mmol, 8.21 g) were placed in a 100 mL three-neck flask at room temperature. The brown solution was heated to 120 °C under vacuum for 20 min to remove water and other impurities with low boiling points. The mixture was then heated to 310 °C and stirred at this temperature for 30 min under N_2. The transparent solution

gradually became turbid starting from 280 °C. Then the mixture was left to cool to room temperature under N_2. The nanoparticles were isolated using ethanol and washed at least three times using a THF/ethanol (1/5) mixture to remove the remaining reagents and organic matter. After the work-up stages, the final product was a yellow paste that could be dried under N_2 to give a yellow powder. The yield of the synthesis vs. the lanthanide is quantitative, as discussed in a previous work.[21] The XRD of the nanoparticles can be found in the Figure S1 of the Supporting Information. The nanoparticles exhibit a hexagonal anisotropic shape with an average width of 10 nm and an average thickness of 2 nm, as will be discussed in the Result section (see Figure 1A for the corresponding TEM).[20]

Nanoplates of Gd_2O_2S of similar morphology and crystallinity were also used for preliminary studies in different parts of this work. They were prepared with a similar protocol, by replacing the cerium precursor by the same molar amount of Gd precursor.

Preparation of the colloidal dispersions (from 10 mg/mL to 70 mg/mL)

Colloidal suspensions of $Gd_{1.9}Ce_{0.1}O_2S$ were obtained by dispersing the paste obtained after the washing steps in a mix of solvent. As a reference sample, we dispersed 200 mg of the paste in ca 4 mL of solvents (in total). The best combination of solvents was found to be CH_3THF and butanol. First, 3.6 mL of CH_3THF was added to the paste, immediately giving an orange colloidal suspension. The suspension was sonicated for 5 min to remove any agglomerates and 0.4 mL of butanol was added. The obtained colloidal dispersions varied from yellow for diluted suspensions (10 to 30 mg/mL) to orange for more concentrated suspensions (40 to 70 mg/mL) and were stable for several months.

Thin film preparation

Films were deposited from colloidal-based suspensions using dip-coating. Several dip-coating parameters were optimized: the temperature of the solution, the withdrawal speed, the chamber relative humidity. For further analysis most of the films were realized on silicon for

UV ellipsometric spectroscopy and on Si/Ti/Cr for IR ellipsometric spectroscopy but as discussed in the supplementary information, the process is applicable to others substrates such as FTO-coated glass slide. The reservoir used for the colloidal suspension was a cylindrical Teflon cuvette with a parallelepiped 2x4 cm hole filled liquid up to 0.5 cm from the top. [25] $Gd_{1.9}Ce_{0.1}O_2S$ coatings were realized thanks to single-layer or multi-layer deposition with a final thickness from a few nm up to 100 nm from the same initial suspension. It should be noted that in this article, "single layer" does not mean a layer of the thickness of a single nanoplate, but rather, that a single deposition was made (one dip in, one dip out). The colloidal suspension was cooled down in a 4 °C fridge for 15 minutes before use. The atmosphere in the dip-coating chamber was kept under low relative humidity (< 10%) using N_2 flow. A layer of the non-volatile species was obtained above the drying line in a few seconds due to the use of very volatile solvents leaving a few nm thick layer on the substrate.

Single layer deposition

The substrate was dipped in the solution and then withdrawn at a given withdrawal speed. Depending on the concentration of the solution (from 12.5 mg/mL to 70 mg/mL) and on the withdrawal speed (from 0.5 mm/s to 10 mm/s), we obtained films from a few nm to 70 nm following a one-layer deposition, as discussed below.

Multi-layer deposition

The multi-layer process involves several successive depositions. As the solvents evaporated quickly from the film, we just let the first layer dry for a few seconds before dipping it again into the suspension: no intermediate thermal treatment was necessary, in contrast with other works.[26,27] Here, the suspension already contained fully formed nanoplates, which allowed the next layer to be directly deposited on the previous one in order to obtain thicker films.

Characterizations

TEM. Transmission Electron Microscopy images were collected with a TWIN 120 (TECNAI SPIRIT) instrument at 120 kV and with a JEOL 100CF apparatus. The grids were prepared as follow: a drop of diluted solution of $Gd_{1.9}Ce_{0.1}O_2S$ dispersed in pure THF was allowed to dry on an amorphous carbon-coated copper grid. TEM images of the suspensions were made using a 20 µL micropipette. The mean size was obtained here using ImageJ software. The command "analyze particle" is used to count and measure objects in thresholded images. For this automated analysis, we assumed all geometries of aggregate are ellipsoidal with circularity ranging from 0 to 1. Mean size values are expressed in physical size units (here nm) and corresponds to the mean diameter of the objects.

SEM. Morphology of the film was observed through **Scanning Electron Microscopy** (SEM). Nanoscale was achieved thanks to a Hitachi SU-70 FESEM (Schottky type gun) operated at 15 kV. Typical resolving power is 1 nm at this accelerating voltage but actual resolution measured through image analysis software is 2.5 nm.

XRD. The **X-ray diffraction pattern** of dry powder was measured on a Bruker D8 diffractometer using Cu Kα radiation at 1.5406 Å. Typical diffractograms were collected with steps of 0.05° and a scanning speed of 5 s/point. The backgrounds of the patterns were subtracted using the EVA software. Grazing incidence XRD data were collected on a laboratory 5-circles diffractometer (Rigaku SmartLab) with Cu Kα radiation (wavelength of 1.54 Å).

Spectroscopic Ellipsometry. The refractive index and the thickness of final films were measured, after the thermal treatment, by **spectroscopic ellipsometry** performed on a UV-NIR (193−1690 nm) variable angle spectroscopic ellipsometer (VASE) M2000DI from Woollam at an incidence angle of 70 °, and the data analysis was performed with the CompleteEASE software. Data were fitted to an appropriate model composed of a Si substrate, a native oxide layer, a SiO_2 and a B-spline layer representing our material with

variable thickness and optical constants. The Mean Squared Error (MSE) was employed to quantify the difference between the experimental and model generated data. Generally, MSE < 15 is considered a good agreement between modeled and measured data.

UV-Vis. UV-Vis absorption spectra of the suspensions were recorded on a Varian-Cary 5E spectrometer from 300 to 800 nm using 70 μL UV quartz cells.

DLS. The size distributions of the colloids in the colloidal suspensions were measured by DLS using a Malvern Zetasizer Nano ZS90 (Malvern Instruments Ltd, Worcestershire, UK) equipped with a 4 mW He–Ne laser at a wavelength of 633 nm. Measurements were made at 25 °C with a fixed angle of 90 ° with a total of three acquisitions of 15 measurements per sample.

Results and Discussion

Optimization of the solvent mixture for colloidal suspension of $(Gd,Ce)_2O_2S$ nanoparticles

At the end of the synthesis, the nanoplates were hydrophobic as surrounded by oleate chains.[23] The nanoplates also tended to aggregate and form lamellar superstructures.[28] It was challenging to disperse them in a mix of solvents, convenient for dip-coating purposes, where they could be stable as a suspension. A preliminary analysis on Gd_2O_2S nanoplates showed that dispersing the paste obtained after the washing steps facilitates the dispersion of the nanoparticles rather than dispersing the dried powder (see Figure S2). Several solvents (water, hexane, THF, dioxane, butanol, propanol) and solvent mixtures, THF/dioxane (*v/v* = 9/1, 8/1, 7.5/2.5) and THF/butanol (*v/v* = 9/1, 8/1, 7.5/2.5), were investigated, with two criteria: the suspension had to be stable for at least 24 h, and the quality of the film obtained by dip-coating had to be optical (i.e. exhibiting no light scattering). This latter point implied both a good wettability of the solution on the silicon substrate, and a moderate solvent evaporation speed. This implies for the mix of solvents to be volatile enough to dry within a few seconds, viscous enough to cover the substrate, and with a low surface tension. THF was already known as a good solvent to form stable dispersion of the nanoparticles. Alcohols (EtOH in particular) are usually appropriate solvents for dip-coating because they have low surface tension and are fairly volatile, which promotes easy spreading of the solution and relatively fast evaporation. THF and butanol mixtures were thus identified as good candidates. Because THF present a fairly high toxicity as it is a monomer easily absorbed by all routes of exposure, it was then replaced by a greener solvent, 2-methyltetrahydrofuran (CH_3THF). Finally, the optimized combination of solvents was CH_3THF and butanol (*v*/*v*=9/1). The as-prepared colloidal dispersion was stable for several months. We showed that the individual nanoparticles were intact in the suspension after 1 month. Figure 1 shows the transmission electron microscopy images of the as-prepared nanoparticles after washing, drying and

dispersed in THF (A) and of the paste of nanoparticles dispersed in the optimized mix of CH_3THF and butanol (B). The shapes and average sizes (10 nm wide and 2 nm thick) were identical in both cases. The platelets are either lying on the side showing the {100} facet or flat showing the {001} facet. The random crystalline orientation of the nanoplates did not influence the formation of the film, as they are covered with a layer of organic ligands.

Interestingly, the nanoparticles in the optimized mix of CH_3THF and butanol tended to aggregate in large agglomerates of diameter around 80-100 nm (Figure 1C, an aggregate is circled in white dotted line).

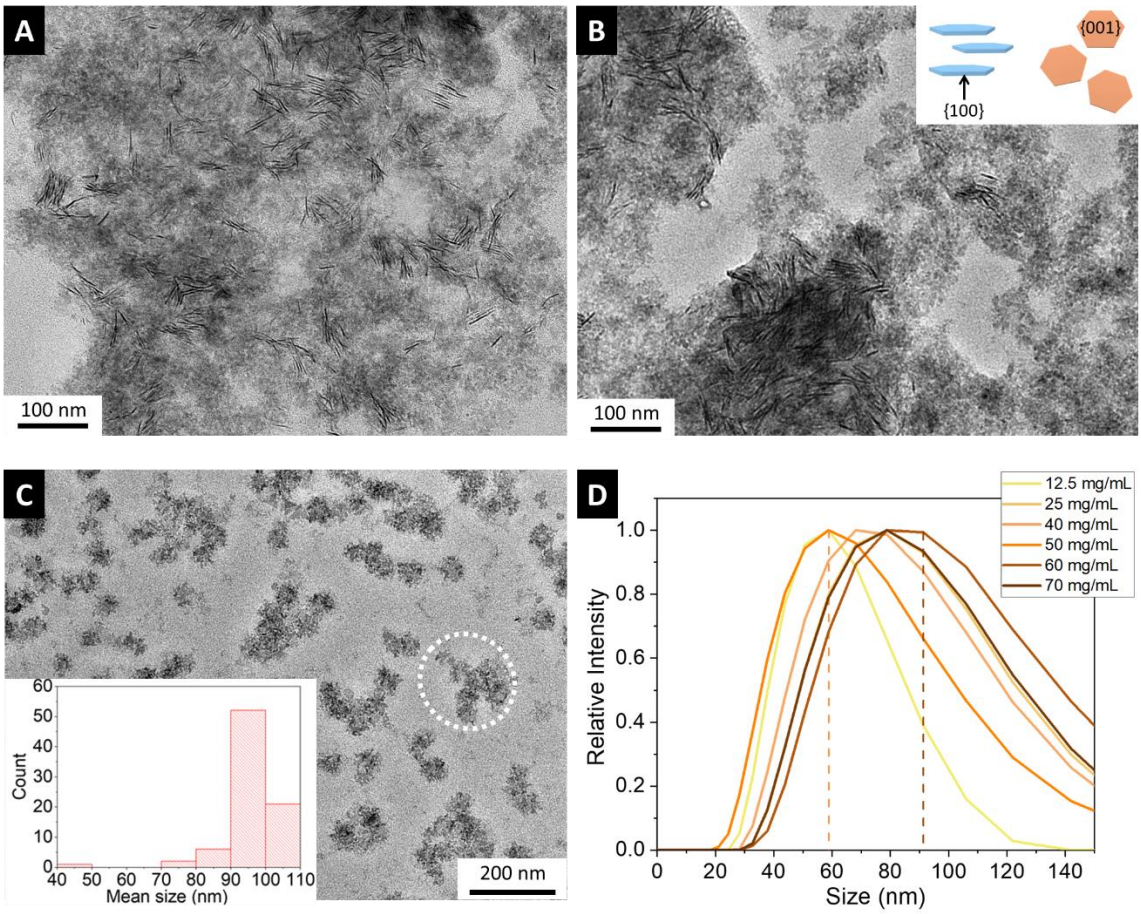

Figure 1 : TEM images of $Gd_{1.9}Ce_{0.1}O_2S$ nanoparticles (A) as-prepared and (B) from the colloidal suspension of CH_3THF/ butanol (v/v=9/1) (the inset is a scheme of the nanoplates indicating their crystallographic orientation). Darker regions correspond to nanoparticles lying on their {100} facet and lighter region corresponds to flat nanoparticles showing their {001} facet. (C) TEM image of $Gd_{1.9}Ce_{0.1}O_2S$ nanoparticles from the suspension in CH_3THF and butanol (the inset corresponds to the size distribution of the aggregates). White dotted line is a

guide to the eye. (D) Average hydrodynamic diameter of the aggregates of colloidal suspensions from concentration of 12.5 to 70 mg/mL.

In order to characterize these stable aggregates, we performed dynamic light scattering experiments on the suspensions of the whole concentration range, from 12.5 to 70 mg/mL (Figure 1D). This provided average hydrodynamic diameters of ca 60 nm (for the more diluted suspension) to ca 90 nm for the majority of the suspensions. This ensemble observation was consistent with the aggregates observed by TEM. The aging of the solution was also investigated through DLS, TEM and UV-Vis absorbance spectroscopy. Figure S3C shows an increasing average hydrodynamic diameter of the aggregates over time for the same suspension at 50 mg/mL (from 60 nm on the day of the synthesis to 80 nm after 30 days). This analysis was completed by TEM images (see Figure S3A and S3B) where the aggregation state of the nanoparticles was clearly observed after 30 days. Nanoparticles tended to pile up and form bigger superstructures. In Figure S3C, UV-Vis absorbance spectroscopy was used to follow the absorbance of the colloidal suspensions. As expected, due to aggregation the absorbance decreased over time and the peak was slightly shifted towards larger wavelength (from 226 nm to 235 nm).

Overall, the suspensions were displaying a two-scale structure. The first one has the typical width of the individual nanoparticles. Because these are anisotropic, in the shape of nanoplates, the packing is not expected to be very compact at this scale, generating a porosity in the range of a few angströms. The other structure is at a broader typical length of ca 80 nm, coming from the formation of stable aggregates in the suspension. At room pressure, the deposition of these aggregates is expected to result in fairly large pores between them, with a broadness of a few nm. Using fresh colloidal suspensions would allow us to get more homogenous films as they are less aggregated compared with aged suspensions. This will be discussed in a later section in relation with the optical index of the thin films.

Film deposition and characterization

Single-layer and multi-layer thin film of $(Gd,Ce)_2O_2S$ on silicon, FTO and kapton substrates

Dip-coating is an ideal method to prepare thin layers from chemical solutions because of its simplicity and easiness to operate. Moreover, it offers a relatively fair control over the thickness, while being compatible with flexible substrates.[29] Despite its apparent simplicity, it involves a complex interplay between several critical parameters including the withdrawal speed, viscosity and evaporation speed (meaning a sensitivity to the temperature and the relative humidity in the chamber).[25] The uniformity and thickness of the coating are also dependent on the concentration and the solvents used for the colloidal suspension. The first parameter to control was the role of the solvent relative vapor pressure in the atmosphere during dip-coating, especially using a volatile solvent such as CH_3THF.[25] In order to minimize the CH_3THF solvent vapors during the film formation, the colloidal suspension was cooled down in a 4 °C fridge. The optimized withdrawal speed was 2 mm/s as it provided homogenous thin films in a reproducible manner.

With these process parameters, single layer (meaning, only one deposition step) thin films of $Gd_{1.9}Ce_{0.1}O_2S$ nanoplates aggregates were deposited on Si/Ti/Cr substrates using a colloidal suspension at a concentration of 50 mg/mL. Ellipsometric measurement was used for characterizing the film thickness. The as-made single layer film on Si/Ti/Cr substrates is shown in Figure **2**A and its thickness was 30 nm. The as-made 5-layer film on Si/Ti/Cr substrates (Figure 2B) was of optical quality and presented a color varying from blue to orange. These colors were structural and were related to the film thickness and refractive index, the top of the film was blue and corresponds to the thickest part (99 nm) and the bottom was orange and corresponds to a slightly lower thickness (75 nm). Finally, Figure **2**C shows a calcined 5-layers thick film on Si/Ti/Cr substrates (as will be discussed in a later

section) and the resulting thickness was 40 nm. In addition to rigid substrates, flexible substrate such as a band of kapton could also be used. Such a film was obtained under similar operating conditions and was of optical quality as well, as showed on Figure 2D. Thanks to the mild temperature required for the film, we were also able to calcine this film while preserving the integrity of the kapton substrate (Figure 2E). We confirmed the presence of the film on kapton after calcination by optical microscopy, we clearly see the delimitations of the different deposition cycles (Figure 2F).

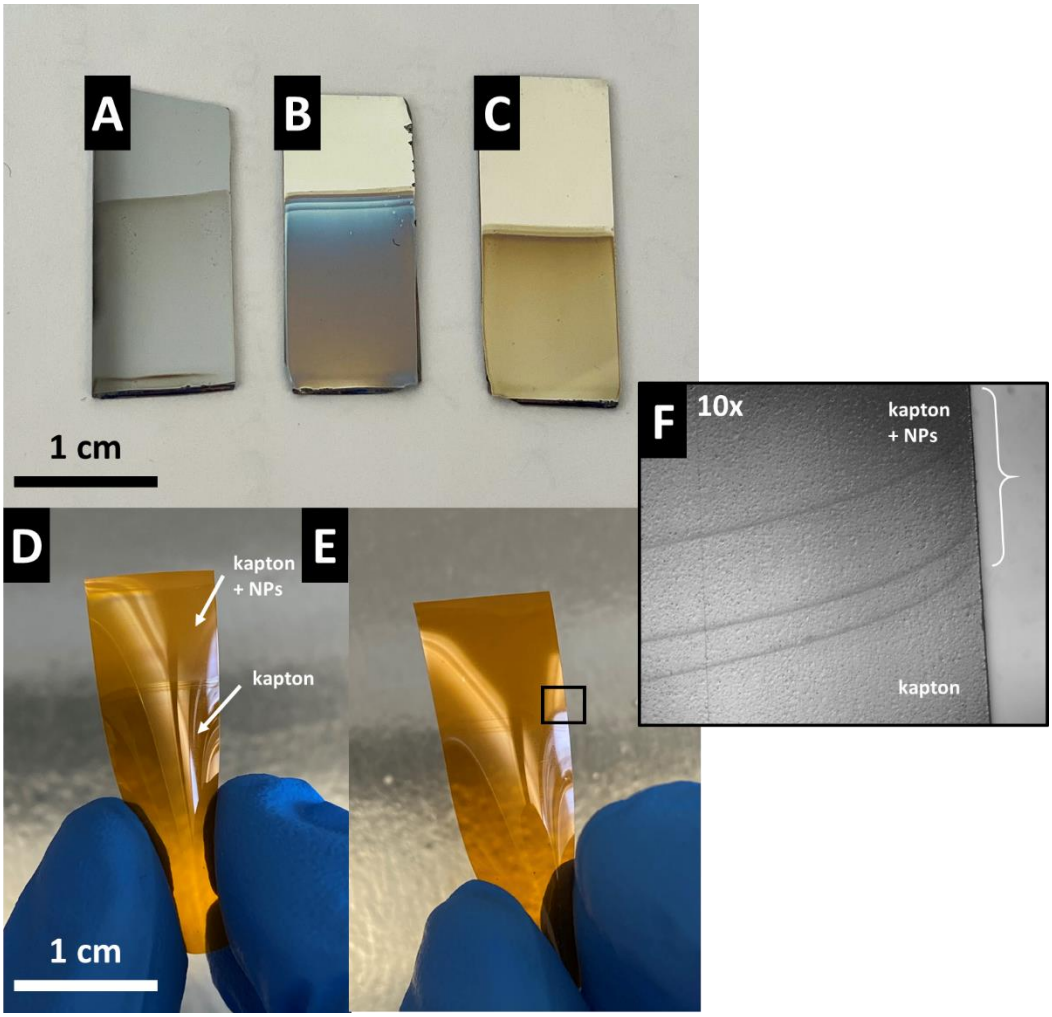

Figure 2 : (A-C) Picture of thin films of a 50 mg/mL $Gd_{1.9}Ce_{0.1}O_2S$ suspension dip-coated on Si/Ti/Cr substrates at 2 mm/s: (A) as-made single layer (B) as-made multi layers (5 layers) and (C) calcined 1 min at 350 °C multi layers (5 layers). (D) Picture of a thin film (10 layers) of a 50 mg/mL $Gd_{1.9}Ce_{0.1}O_2S$ suspension dip-coated at 3 mm/s on kapton, a flexible substrate, before calcination. (E) Picture of the same film after 1min at 350 °C. (F) Optical microscope image (x10) of the calcined kapton film showing the resulting film and the different deposition cycles.

In order to analyze the films at the microscale, the morphology of a representative film was observed using Scanning Electron Microscopy. A single-layer film deposited on a silicon substrate from a Gd_2O_2S colloidal suspension at 50 mg/mL is showed on Figure 3A. The surface of the substrate was mainly covered by the nanoplates which kept their original size and shape. The thickness of the thin-films was characterized by observing a cross section of the film (Figure 3B). The thickness varied between 28 and 41 nm in the observed region (ca 500 nm wide), with an average value of 37 nm. This was representative of other regions of the thin films. This thickness was consistent with these obtained by ellipsometric measurement: 34 nm. Similar images were realized on FTO glass substrate and are presented in Figure S4. The average thickness of the film and the size of the nanoplates are identical on silicon and on FTO.

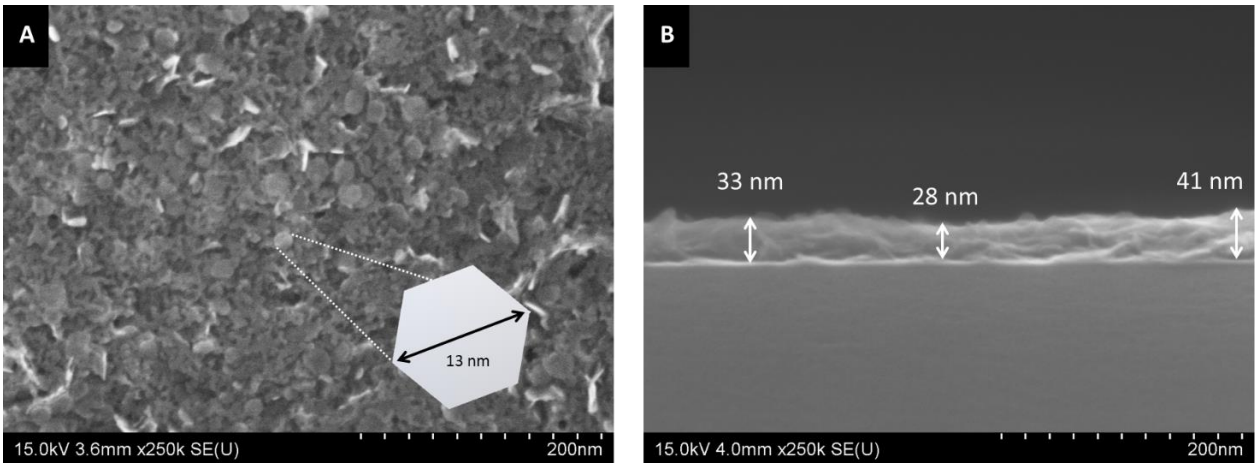

Figure 3 : SEM-FEG images of (A) top view and (B) cross section of a single-layer Gd_2O_2S thin film on Si substrate, from a colloidal suspension at 50 mg/mL. The scheme in (A) indicates the width of a selected nanoplate lying flat on the surface.

Preliminary experiments with more diluted (down to 12.5 mg/mL) and more concentrated (up to 70 mg/mL) suspensions, as well as with Ce-containing $Gd_{1.9}Ce_{0.1}O_2S$ nanoparticles showed that the optimized parameters allowed the deposition of optical-quality thin films. The deposition can be applied to other kind of substrates and as seen on the Figure S5.

$Gd_{1.9}Ce_{0.1}O_2S$ nanoparticles were successfully deposited on FTO coated glass leaving a homogenous orange thin layer.

In the next section, we will discuss how to tune the thickness of the films. Ellipsometric measurements provides the film thickness as an average over a mm scale, with a few minutes in a non-destructive manner, and it is more appropriate to characterize series of thin films and will be used as the preferential method in the rest of the article. Only $Gd_{1.9}Ce_{0.1}O_2S$ nanoparticles will be discussed as they present a higher interest for further applications.

Thin films of $Gd_{1.9}Ce_{0.1}O_2S$ nanoplates with tunable thickness on silicon substrates

Two main levers were used to tune the thickness: the withdrawal speed and the concentration of the nanoplate suspension. In both cases, the main constraint was the formation of a homogeneous layer that is thick enough to undergo a thermal treatment as discussed in the next section. Additionally, thicker films were then grown using a multi-layer strategy.

We investigated first the effect of the withdrawal speed. Figure 4A shows the different thicknesses obtained from a single-layer thin film of a 50 mg/mL $Gd_{1.9}Ce_{0.1}O_2S$ suspension on Si substrate. The most homogeneous films were obtained between 2 and 4 mm/s withdrawal speed. The obtained thicknesses (35 to 55 nm) are sufficient to go through a thermal treatment as we expected the thickness to drop due to the loss of ligands.

The second method used to control the thickness was from the concentration of the colloidal suspension (Figure 4B): more concentrated ones are expected to lead to thicker films, as there are more nanoplates to be deposited. A range of suspensions of $Gd_{1.9}Ce_{0.1}O_2S$ nanoparticles was prepared with concentrations of 12.5, 25, 30, 40 and 70 mg/mL. The full dots on Figure 4B (labeled “as made”) show the thicknesses of thin films prepared with these suspensions. The values range from 10 to 88 nm and increased with the concentration, as expected. Yet, if

the increase is fairly linear up to 30 mg/mL concentration, higher concentrations barely lead to higher thicknesses. Dip-coating theory teaches us that this effect can be due to either a strong viscosity and/or surface tension decrease, or to solution concentration not increasing as much as expected[25]. The latter hypothesis is likely to be the main phenomenon at play here because DLS analyses proved that colloids aggregates are larger for the high concentrations of solutions, so that a part of colloids may have sedimented at the bottom of the dip-coating cuvette. Using high concentration of solution for getting high film thickness is thus a limited strategy so far, unless a study dedicated to the stabilization of these colloids at high concentration is engaged.

A third strategy to tune the thickness was to deposit multilayer films. As discussed in the experimental section, after a few seconds of drying in air, the layers were adhesive enough to withstand being dipped in the suspension again: no intermediate calcination or consolidation was required. This is a very convenient advantage to form multilayer films. Three intermediate concentrations were selected for this study: 30, 40 and 50 mg/mL. Thus, we formed multilayer films by successive dipping of the substrate several times in the colloidal suspension. The thickness was measured between each deposition by the non-destructive ellipsometric measurement. The full dots of Figure 4C show the thickness of the thin films for each of the two concentrations. For 30 mg/mL, the first layer provided a 24 nm thick film. Then, successive thicknesses of 48, 73, 94 and 110 nm were obtained respectively for layers number 2, 3, 4 and 5. This corresponds to a quasi-linear trend where each layer adds 23 nm to the overall thickness (Figure S6). A similar trend was found for the concentrations of 40 mg/mL and 50 mg/mL, with successive thicknesses from 26 to 128 nm and from 34 to 135 nm. Although the trend was less regular, this corresponded roughly to 27 nm per layer for 40 mg/mL and 30 nm for 50 mg/mL, both values slightly higher than these obtained at 30 mg/mL.

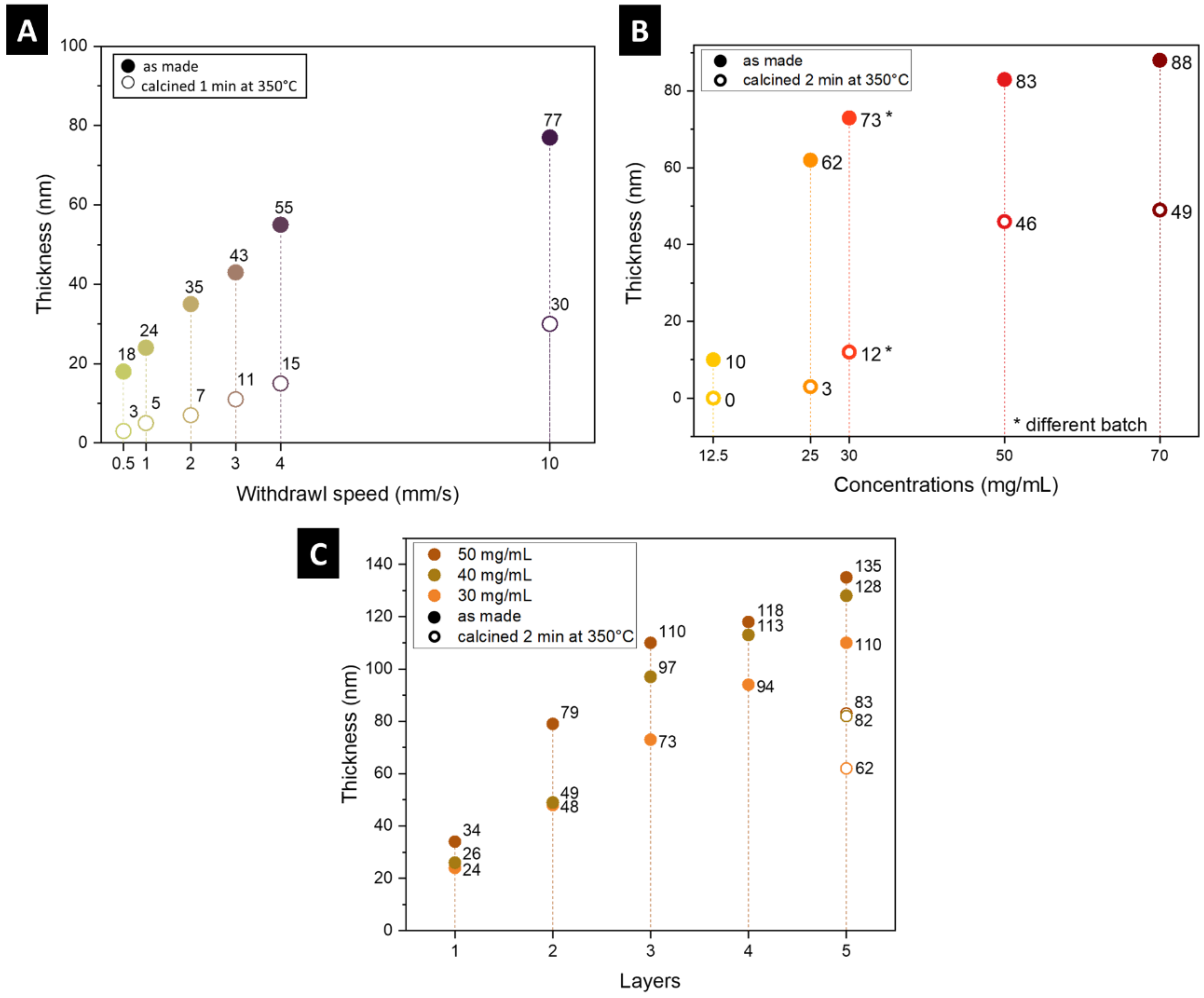

Figure 4: (A) Thickness of a single-layer from a 50 mg/mL colloidal suspension of $Gd_{1.9}Ce_{0.1}O_2S$ nanoparticles at different withdrawal speeds on Si substrate. (B) Thickness of a three-layer thin films as a function of the concentration of the colloidal suspension of $Gd_{1.9}Ce_{0.1}O_2S$ nanoparticles. (C) Thickness of the thin films as a function of the number of layers, for three selected concentrations: 30, 40 and 50 mg/mL.

Another point should be commented at this stage: when comparing data from (B) and (C) we remark differences between the thicknesses obtained from (B) for three-layer films and the thicknesses read at layers = 3 in (C). Indeed for 30 mg/mL, the values match (73 nm), but for 50 mg/mL, the value tends to be higher: 110 nm in (C) *vs* 83 nm in (B). This might be due to the fact that in (C), the measurement of the thickness after every layer obliged us to remove the film from the dip-coating chamber and pass it through the ellipsometer beam. The film was then allowed to dry under ambient atmosphere for a longer time compared to the multi-layer process where layers are successively deposed. Moreover, as the films were made up of

different nanoparticles batches, we cannot guarantee that each single dispersion behaves strictly the same due to expected differences at the end of every synthesis arising from the yield and the ability of the nanoplates to assemble together.

For comparison purposes, aged suspensions were used to deposit thin films and pictures of the obtained samples are presented in Figure S7. As expected from previous DLS and TEM analysis (Figure S3), the suspensions after 30 days did not give homogenous films and the thickness obtained was much lower from what we previously got with recent suspensions. This confirms the importance of working with freshly prepared colloidal suspension in order to get the most homogenous and thick films.

Overall, the optimized dip-coating process provided three opportunities to tune the film thickness, from 10 to 135 nm, as shown here. While the concentration of the suspension cannot be increased to much higher values due to the lack of stability of the resulting colloids, it should be noted that there is no limitation, *a priori*, to the number of layers that could be deposited in the multi-step process. We checked for the upper limit of film deposition by doing up to 30 deposition cycles on Si. The thickness increases linearly with the number of layers as presented in Figure S8. Thus, thicker films may be obtained, would the targeted application demand it.

Thermal treatment of the thin films

As a result of the synthetic protocol, the nanoparticles were surrounded by hydrophobic oleate chains,[23] which were still present in the colloidal suspension in the mixture of CH_3THF and butanol. Thus, the nanoplates and the film were still hydrophobic after the dip-coating step performed at room temperature. Removing the hydrophobic chains of the nanocrystals would make them suitable for practical use, e.g. in water or biological media. Moreover, it would make the surface of the nanoparticles available to interact with adsorbates by opening the

inter-particular and inter-aggregates spaces that were so far filled with organic surfactants and other remaining adsorbed species such are traces of CH_3THF or butanol.

Here, we aimed at obtaining ligand-free thin films of nanoplates by controlling the thermal decomposition of the ligands in oxidizing atmosphere. A simple yet efficient method to remove organic ligands from supported nanocrystals relies on a fast-thermal treatment during which ligands are quickly degraded before the film starts to sinter. The challenge was to find operating conditions of time and temperature that would desorb the fairly volatile species and degrade the oleate chains without compromising the inorganic structure of the $Gd_{1.9}Ce_{0.1}O_2S$ nanoparticles, e.g. by oxidation of the cerium and/or sulfide.

A previous study based on powder showed that organic species are removed at different stages of the thermal treatment.[23] This was obtained by thermogravimetric analysis performed on a few mg of Gd_2O_2S powder and showed that the inorganic phase is stable up to around 350 °C under oxidizing atmosphere. This temperature was also necessary and sufficient to remove alkane chains from the nanoparticles surface. Here, a moderate temperature range of 300 to 350 °C was used, as detailed below. Moreover, the thermal treatment would have to be short enough to avoid significant sintering of the nanoparticles. Typical duration for thermal treatments of thin films[30–32] are only a few minutes vs. several tens of minutes for regular powders.

As a first step, a 80 nm-thick film of Gd_2O_2S nanoparticles on Si/Ti/Cr was characterized by infra-red spectroscopy. Due to the low amount of material on the film, regular IR spectrometers were not adequate. Rather, we used IR-Variable Angle Spectroscopic Ellipsometry measurement. Figure 5A shows the IR spectra of the thin film before calcination (in blue). We highlight here that this characterization method allows determining the absolute extinction coefficient of a unit volume of material, that is, no normalization is required (i.e. absolute values of extinction coefficients k spectra obtained can be compared). We observed

the CH_2 and CH_3 stretching bands between 2820 and 2970 cm^{-1} on the as-made film corresponding to the oleate ligands, as expected from previous measurements on powders.[23] We also observed COO stretching bands at 1500 and 1375 cm^{-1} and sulfates between 1020 and 1200 cm^{-1} arising from the partial oxidation of the surface of nanoparticles when exposed to air.[21]

Because this measurement was non-destructive, the effects of the thermal treatment on the environment of the nanoparticles could be investigated on the very same film after calcination of the ligands. The thermal treatment was performed at 315 °C for 1 min. Figure 5 shows in orange the IR spectrum after the thermal treatment. CH_2 bands were not present anymore and SO_4^{2-} signals was considerably reduced, meaning that this calcination was an efficient way to remove organic ligands.

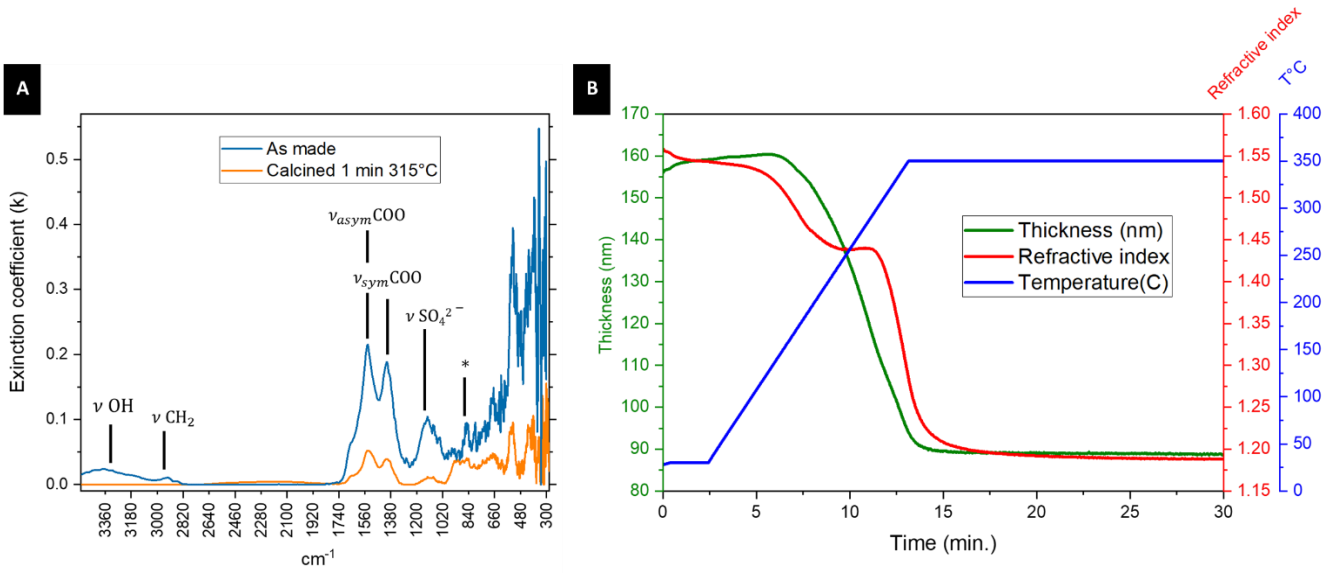

Figure 5 : (A) IR-VASE experiments on as-made and calcined three-layer thin film of Gd_2O_2S nanoparticles on Si/Ti/Cr substrates. (B) *in-situ* UV-NIR VASE experiment at 600 nm on a three-layer $Gd_{1.9}Ce_{0.1}O_2S$ thin film on Si.

In order to refine the thermal treatment and to monitor the optical constants that are related to the thin film, an *in-situ* UV-VASE experiment was realized by coupling a heat cell to the ellipsometer. This experiment was performed on a three-layer $Gd_{1.9}Ce_{0.1}O_2S$ thin film deposited on Si, with a thickness of 130 nm. During this experiment, the heat cell was

connected to an aluminum plate on which the substrate was put. The plate was heated from 30 °C to 350 °C at a rate of 32 °C/min, then the temperature was kept at 350 °C for 15 min. The evolution of the optical constants including the thickness of the film and the refractive index were recorded and displayed on Figure 5B.

From 5 to 13 min, which corresponds to the heating ramp, the film thickness decreased by half from ca 130 nm to 70 nm. The film was contracted in the direction perpendicular to the substrate as a consequence of the loss of organic ligands and volatile species, consistently with observations made on a broad range of materials, such as zirconia sol-gel thin films that tend to shrink as heat treatment proceeds and dry as a porous structure before complete densification at higher temperature (700 °C).[33] After 15 min and at the temperature of 350 °C, the film thickness only slightly decreased, indicating that most of the volatile species were already lost before.

The loss of organic ligands corresponds to a modification of the film composition toward the denser inorganic phase, but should also liberate a significant amount of porosity, as the nanoplates are not expected to be densely packed.

Another way to analyze the film composition is to monitor the refractive index at a given wavelength (here, 600 nm). For large crystals of Gd_2O_2S, it is expected to be approximately 2.1-2.3.[34] After collecting experimental parameters by spectroscopic ellipsometry, a model-based approach was used to determine the Cauchy's refractive index. The value evaluated on the film before treatment was ca 1.55, much lower that these of the pure material. This was due to the present of lower index species in the thin film: oleate ligands, remaining volatile molecules, and interparticular porosity.

Variations of the refractive index were observed as a consequence of the thermal treatment. In a first stage, at the beginning of the heating ramp (4 to 7 min), it slightly decreased, suggesting that the film was less dense. This could be due to the desorption of physisorbed

volatile solvent molecules from the film. Then, from 7 to 12 min, the refractive index stays stable. This already corresponded to a strong decrease of the thickness of about 30 %, down to 95 nm. At this stage, it is possible that the Van-der-Walls interaction between the organic chains of the oleates were stronger, in the absence of solvent molecules, which resulted in increasing the density of the film. Then, from 12 to 15 min, while the film thickness was still strongly decreasing, the refractive index swiftly dropped down to 1.26. We interpret this as the degradation of the oleate chains into volatile species, which liberates the porosity of the film and decreases its average density. On the temperature plateau, from 15 to 30 min, the index stays stable at 1.2, suggesting no major changes in composition or porosity but a mere densification of the film.

Overall, this *in situ* experiment allowed confirming that 350 °C was an adequate and sufficient temperature to remove the oleate chains as well as other volatile species from the thin film, within a few minutes. As an example, a picture of a multi-layer film that has undergone calcination at 350 °C for 1 min is showed in Figure **2**C. The structural colors disappeared due to the removal of organic ligands and consequently to the thickness decrease.

We further verified this by applying a calcination at 350 °C for 2 min on selected films presented in the previous section, and we monitored the consequence of calcination on the film thickness. In Figure 4A and B, the open circles represent the thickness of the thin films after this thermal treatment. Thickness decrease in the same order of magnitudes were observed as a result of this *ex situ* treatment. It should be noted that for the *ex situ* treatment, the thin film was placed in a pre-heated oven at 350 °C where the temperature was monitored by a PID controller. Unlike for the ellipsometry *in-situ* experience, it allowed a direct thermal treatment at a given temperature without any heating ramp. For instance, the 130 nm-thick film on Figure 4B resulted in a 83 nm-thick film after calcination. Similar results were obtained regardless of the initial thickness of the number of layers deposited. This suggested

that the porosity could be generated within the full thickness of the film, down to the substrate.

As mentioned before, the optimized thermal treatment would allow the departure of the ligands, which we verified so far, but this should be done without altering the physico-chemical properties of film, including the morphology of the nanoparticles by avoiding sintering and their crystalline phase.

In order to verify that the nanoplates conserved their integrity during the thermal treatment, a TEM grid was prepared from debris of a scratched calcined thin film, slightly dispersed in EtOH. Figure 6B showed nanoparticles with the same morphology than the staring ones, confirming that no significant sintering was occurring. The same process was done on FTO coated glass and TEM images are shown in Figure S9. It should be noted that on FTO and after thermal treatment, the nanoplates tended to pile up perpendicularly to the substrate.

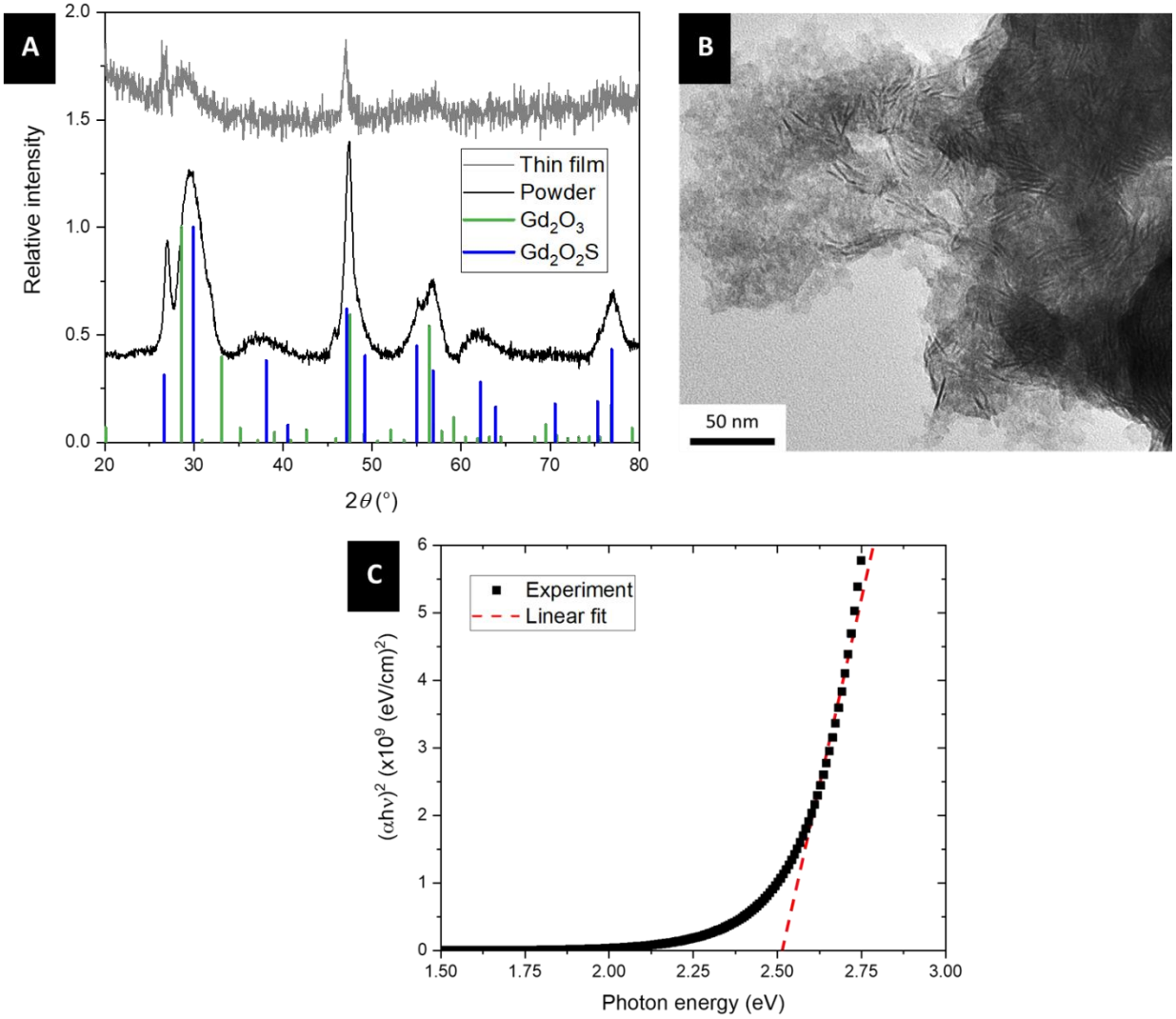

Figure 6 : (A) X-Ray diffraction of a three-layer $Gd_{1.9}Ce_{0.1}O_2S$ thin film on Si at a grazing incidence of 0.3 ° (in grey) in comparison with the pattern of a powder of $Gd_{1.9}Ce_{0.1}O_2S$ (in black). The original data recorded at grazing incidence were binned (N=3) to while the intensity was recorded every 0.05 ° in the raw data. Green peaks correspond to Gd_2O_3 (PDF 00-012-0797) and blue peaks correspond to Gd_2O_2S (PDF 00-026-1422). (B) TEM image of a three-layer $Gd_{1.9}Ce_{0.1}O_2S$ thin film on Si, calcined for 2 min at 350°C. TEM grid was prepared from debris of the film in EtOH. (C) Tauc plot of $Gd_{1.9}Ce_{0.1}O_2S$ thin film calcined 2 min at 350°C.

Moreover, the film was too thin for regular XRD to provide information regarding the crystallinity of the nanoparticles. Thus, grazing incidence X-Ray diffraction, more sensitive, was performed and the pattern is showed on Figure 6A in grey color. The signal-to-noise ratio was still poor but the diffractogram was compared with these of the corresponding powder of nanoparticles (in black color), as well as with the reference of the hexagonal phase of Gd_2O_2S. Overall, the peaks detected at 26 and 76 ° are consistent with the presence of a crystalline

phase isostructural to Gd_2O_2S which appears to be the major specie at the surface of the substrate. Moreover, Figure 6C shows the Tauc plot of a calcined thin film of $Gd_{1.9}Ce_{0.1}O_2S$, i.e., $(\alpha hv)^n$ versus hv curve which enables estimation of the band gap. The values were obtained from the Tauc relation $\alpha = \frac{4\pi k}{\lambda} = K(hv - E_g)^n$ with α the absorption coefficient, k the extinction coefficient obtained from spectroscopic ellipsometry, K a constant and E_g the band gap. This model is parameterized by a power n which depends on the type of band gap. In recent reports on Ln_2O_2S compounds, it was argued that the band gap is direct, which corresponds to $n = 2$. [20,35,36] The linear portion of the curve was extrapolated to the X-axis and the optical band gap energy of the corresponding thin films was obtained from the intercept, following the method presented by Makula et al.[37] Using the Tauc plot approach, the optical band gap was found to be 2.5 eV, which corresponds to the Gd_2O_2S oxysulfide phase doped with 5% of Ce.[20] For comparison the bandgap of Gd_2O_3 is around 5 eV.[38]

Altogether, the thermal treatment proposed in this section allowed to remove the oleate ligands and to generate porosity in the film while preserving the structural integrity of the nanoplates. This was verified in details for a 3-layer 130 nm-thick film and reproduced on thin films of initial thicknesses from 10 to 135 nm, showing the robustness of the process. The optical quality of the film was confirmed by the low level of depolarization during the spectroscopic ellipsometry experiments, making them suitable in any optical set up as far as we can say. In addition, we measured the complex optical dispersion law of our material. This includes extinction coefficient k(lambda) of our materials (which is homogeneous with an optical density) with accuracy. The dispersion law of our film after calcination (including real part of refractive index n and imaginary part k accounting for absorption properties of the film at high energy) can be seen in Figure S10.

Conclusion

In the present study, we showed the preparation of optical-quality thin films from suspension of nanoplates prepared *via* a colloidal method. The thickness of the film was tunable from single to multi-layers and a thermal treatment was applied to remove the remaining ligands at the surface of the nanoplates. Here we focused on the quality of the deposition as well as its characterization from the colloidal synthesis, to the dispersion and deposition and finally to the calcination. The results of morphological studies showed the preservation of the shape and size of the nanoparticles. This study also highlights the fact that realizing thin films from colloids requires to have a sound appreciation of different key parameters including the dispersion of the nanoparticles, the stability and aging of the suspension, its ability to cover the substrate and to undergo thermal treatment. Our results open the way for the design of lanthanide oxysulfide coatings on a variety of substrates, including flexible ones, as illustrated on kapton. Moreover, the optimized protocol described here can be easily applied to any other mono- or bi-cationic lanthanide oxysulfide nanoplates, for which we already provided detailed synthesis protocols and characterization in our previous studies. As a consequence, the present work opens an avenue to the unprecedented utilization of optical-quality thin films of Ln_2O_2S nanoparticles for a range of optical applications, eg. in laser technologies.

Supplementary Materials

Additional TEM and SEM-FEG images, DLS measurements, pictures of colloidal suspensions and thin films, XRD analysis, linear fit of the thickness vs. the number of layers.

Acknowledgments

Sorbonne Université is acknowledged for the PhD grant of L. M. David Montero is gratefully acknowledged for conducting SEM-FEG experiments. SEM-FEG instrument was funded by Sorbonne Université, CNRS and Région Ile de France, and is a part of FCMat, The Federation of Chemistry and Materials of Paris-Center. Mohamed Selmane (IMPC) and Yunlin Jacques Zheng (INSP) are gratefully acknowledged for providing the grazing incidence XRD data.

References

(1) Li, Z.; Fan, Q.; Yin, Y. Colloidal Self-Assembly Approaches to Smart Nanostructured Materials. *Chem. Rev.* **2022**, *122* (5), 4976–5067.

(2) Karki, S.; Kim, H.; Na, S.-J.; Shin, D.; Jo, K.; Lee, J. Thin Films as an Emerging Platform for Drug Delivery. *Asian J. Pharm. Sci.* **2016**, *11* (5), 559–574.

(3) Shetti, N. P.; Bukkitgar, S. D.; Reddy, K. R.; Reddy, C. V.; Aminabhavi, T. M. Nanostructured Titanium Oxide Hybrids-Based Electrochemical Biosensors for Healthcare Applications. *Colloids Surfaces B Biointerfaces* **2019**, *178*, 385–394.

(4) Burnside, S. D.; Shklover, V.; Barbé, C.; Comte, P.; Arendse, F.; Brooks, K.; Grätzel, M. Self-Organization of TiO 2 Nanoparticles in Thin Films. *Chem. Mater.* **1998**, *10* (9), 2419–2425.

(5) Alvarado, J. A.; Maldonado, A.; Juarez, H.; Pacio, M. Synthesis of Colloidal ZnO Nanoparticles and Deposit of Thin Films by Spin Coating Technique. *J. Nanomater.* **2013**, *1-9*.

(6) Sastry, M. Nanostructured Thin Films by Self-Assembly of Surface Modified Colloidal Particles. *Curr. Sci.* **2000**, *78* (9), 1089–1097.

(7) Di Mauro, A.; Fragalà, M. E.; Privitera, V.; Impellizzeri, G. ZnO for Application in Photocatalysis: From Thin Films to Nanostructures. *Mater. Sci. Semicond. Process.* **2017**, *69* (March), 44–51.

(8) Mariappan, R.; Ponnuswamy, V.; Suresh, P.; Ashok, N.; Jayamurugan, P.; Chandra

Bose, A. Influence of Film Thickness on the Properties of Sprayed ZnO Thin Films for Gas Sensor Applications. *Superlattices Microstruct.* **2014**, *71*, 238–249.

(9) Lillo-Ramiro, J.; Guerrero-Villalba, J. M.; Mota-González, M. de L.; Tostado, F. S. A.-; Gutiérrez-Heredia, G.; Mejía-Silva, I.; Castillo, A. C. Optical and Microstructural Characteristics of CuO Thin Films by Sol Gel Process and Introducing in Non-Enzymatic Glucose Biosensor Applications. *Optik (Stuttg).* **2021**, *229* (December 2020), 166238.

(10) Hollar, C.; Lin, Z.; Kongara, M.; Varghese, T.; Karthik, C.; Schimpf, J.; Eixenberger, J.; Davis, P. H.; Wu, Y.; Duan, X.; et al. High-Performance Flexible Bismuth Telluride Thin Film from Solution Processed Colloidal Nanoplates. *Adv. Mater. Technol.* **2020**, *5* (11), 2000600.

(11) Lin, Z.; Chen, Y.; Yin, A.; He, Q.; Huang, X.; Xu, Y.; Liu, Y.; Zhong, X.; Huang, Y.; Duan, X. Solution Processable Colloidal Nanoplates as Building Blocks for High-Performance Electronic Thin Films on Flexible Substrates. *Nano Lett.* **2014**, *14* (11), 6547–6553.

(12) Martin, C.; Barker, R.; Watkins, E. B.; Dubreuil, F.; Cranston, E. D.; Heux, L.; Jean, B. Structural Variations in Hybrid All-Nanoparticle Gibbsite Nanoplatelet/Cellulose Nanocrystal Multilayered Films. *Langmuir* **2017**, *33* (32), 7896–7907.

(13) Ali, T.; Lin, J.; Snow, B.; Wang, X.; Elston, S. J.; Morris, S. M. A Thin-Film Flexible Defect-Mode Laser. *Adv. Opt. Mater.* **2020**, *8* (8), 1901891.

(14) Dumarcher, V.; Rocha, L.; Denis, C.; Fiorini, C.; Nunzi, J.-M.; Sobel, F.; Sahraoui, B.; Gindre, D. Polymer Thin-Film Distributed Feedback Tunable Lasers. *J. Opt. A Pure Appl. Opt.* **2000**, *2* (4), 279–283.

(15) Rabbani-Haghighi, H.; Forget, S.; Chénais, S.; Siove, A.; Castex, M.-C.; Ishow, E. Laser Operation in Nondoped Thin Films Made of a Small-Molecule Organic Red-Emitter. *Appl. Phys. Lett.* **2009**, *95* (3), 033305.

(16) Larquet, C.; Carenco, S. Metal Oxysulfides: From Bulk Compounds to Nanomaterials. *Front. Chem.* **2020**, *1-8*.

(17) Sychov, M. M.; Nakanishi, Y.; Nakajima, H.; Gnatyuk, V.; Magami, T.; Kominami, H.; Hatanaka, Y. Properties and Cathodoluminescence of Y[Sub 2]O[Sub 2]S:Eu Thin Films. *J. Soc. Inf. Disp.* **2003**, *11* (3), 499.

(18) Zhu, K.; Ding, W.; Sun, W.; Han, P.; Wang, L.; Zhang, Q. 1.06 Mm Laser Absorption Properties of Sm2O2S Prepared by Flux Method. *J. Mater. Sci. Mater. Electron.* **2016**, *27* (3), 2379–2384.

(19) Sun, W.; Zhu, K.; Xu, H.; Yang, X.; Yu, M.; Li, X.; Wang, L.; Zhang, Q. Enhanced Absorbing Property of Sm2O2S Laser Absorbent by Doping Er3+/Tm3+. *J. Mater. Sci. Mater. Electron.* **2017**, *28* (1), 697–701.

(20) Larquet, C.; Nguyen, A.-M.; Glais, E.; Paulatto, L.; Sassoye, C.; Selmane, M.; Lecante, P.; Maheu, C.; Geantet, C.; Cardenas, L.; et al. Band Gap Engineering from Cation Balance: The Case of Lanthanide Oxysulfide Nanoparticles. *Chem. Mater.* **2019**, *31* (14), 5014–5023.

(21) Larquet, C.; Nguyen, A.-M.; Ávila-Gutiérrez, M.; Tinat, L.; Lassalle-Kaiser, B.; Gallet, J.-J.; Bournel, F.; Gauzzi, A.; Sanchez, C.; Carenco, S. Synthesis of Ce 2 O 2 S and Gd 2(1– y) Ce 2 y O 2 S Nanoparticles and Reactivity from in Situ X-Ray Absorption Spectroscopy and X-Ray Photoelectron Spectroscopy. *Inorg. Chem.* **2017**, *56* (22), 14227–14236.

(22) Luo, Z.; Li, F.; Zhu, Q.; Sun, X.; Li, J.-G. Low-Temperature Green Synthesis of Nanocrystalline La2O2S:Pr3+ Powders and Investigation of Photoluminescence. *J. Mater. Res. Technol.* **2022**, *17*, 2540–2549.

(23) Larquet, C.; Hourlier, D.; Nguyen, A.-M.; Torres-Pardo, A.; Gauzzi, A.; Sanchez, C.; Carenco, S. Thermal Stability of Oleate-Stabilized Gd 2 O 2 S Nanoplates in Inert and Oxidizing Atmospheres. *ChemNanoMat* **2019**, *5* (4), 539–546.

(24) Nguyen, A.-M.; Pradas del Real, A. E.; Durupthy, O.; Lanone, S.; Chanéac, C.; Carenco, S. Risk Analysis and Technology Assessment of Emerging (Gd,Ce)2O2S Multifunctional Nanoparticles: An Attempt for Early Safer-by-Design Approach. *Nanomaterials* **2022**, *12* (3), 422.

(25) Bindini, E.; Naudin, G.; Faustini, M.; Grosso, D.; Boissière, C. Critical Role of the Atmosphere in Dip-Coating Process. *J. Phys. Chem. C* **2017**, *121* (27), 14572–14580.

(26) Hilliard, S.; Baldinozzi, G.; Friedrich, D.; Kressman, S.; Strub, H.; Artero, V.; Laberty-Robert, C. Mesoporous Thin Film WO3 Photoanode for Photoelectrochemical Water Splitting: A Sol-Gel Dip Coating Approach. *Sustain. Energy Fuels* **2017**, *1* (1), 145–153.

(27) Seo, M.; Akutsu, Y.; Kagemoto, H. Preparation and Properties of Sb-Doped SnO2/Metal Substrates by Sol-Gel and Dip Coating. *Ceram. Int.* **2007**, *33* (4), 625–629.

(28) Larquet, C.; Carriere, D.; Nguyen, A.-M.; Le, T. K.-C.; Frogneux-Plé, X.; Génois, I.; Le Griel, P.; Gauzzi, A.; Sanchez, C.; Carenco, S. Unraveling the Role of Alkali Cations in the Growth Mechanism of Gd 2 O 2 S Nanoparticles. *Chem. Mater.* **2020**,

32 (3), 1131–1139.

(29) Gans, A.; Dressaire, E.; Colnet, B.; Saingier, G.; Bazant, M. Z.; Sauret, A. Dip-Coating of Suspensions. *Soft Matter* **2019**, *15* (2), 252–261.

(30) Hou, H.; Hamilton, R. F.; Horn, M. W. Crystallization of Nanoscale NiTi Alloy Thin Films Using Rapid Thermal Annealing. *J. Vac. Sci. Technol. B, Nanotechnol. Microelectron. Mater. Process. Meas. Phenom.* **2016**, *34* (6), 06KK01.

(31) Li, J.; Zhang, L.; Yao, X.; Wang, J. A New and Rapid Heat-Treatment Process for Fabricating Lead Zirconate Titanate Thin Film. *Ceram. Int.* **2004**, *30* (7), 1509–1512.

(32) Kuznetsova, T.; Lapitskaya, V.; Solovjov, J.; Chizhik, S.; Pilipenko, V.; Aizikovich, S. Properties of Crsi2 Layers Obtained by Rapid Heat Treatment of Cr Film on Silicon. *Nanomaterials* **2021**, *11* (7), 1–11.

(33) Nouri, E.; Shahmiri, M.; Rezaie, H. R.; Talayian, F. A Comparative Study of Heat Treatment Temperature Influence on the Thickness of Zirconia Sol-Gel Thin Films by Three Different Techniques: SWE, SEM and AFM. *Surf. Coatings Technol.* **2012**, *206* (19–20), 3809–3815.

(34) Anan, G. V; Gorokhova, E. I.; Demidenko, V. A.; Parfinski, V. A.; Khristich, O. A. Optical Properties of Gd 2 O 2 S-Based Ceramic. *J. Opt. Technol.* **2005**, *72* (January), 58–61.

(35) Som, S.; Choubey, A.; Sharma, S. K. Spectral and Trapping Parameters of Eu3+ in Gd2O2S Nanophosphor. *J. Exp. Nanosci.* **2015**, *10* (5), 350–370.

(36) Bagheri, A.; Rezaee Ebrahim Saraee, K.; Shakur, H. R.; Zamani Zeinali, H. Synthesis and Characterization of Physical Properties of Gd2O2S:Pr3+ Semi-Nanoflower Phosphor. *Appl. Phys. A Mater. Sci. Process.* **2016**, *122* (5), 1–8.

(37) Makuła, P.; Pacia, M.; Macyk, W. How To Correctly Determine the Band Gap Energy of Modified Semiconductor Photocatalysts Based on UV-Vis Spectra. *J. Phys. Chem. Lett.* **2018**, *9* (23), 6814–6817.

(38) Kuznetsova, Y. A.; Zatsepin, A. F. Optical Properties and Energy Parameters of Gd 2 O 3 and Gd 2 O 3 :Er Nanoparticles. *J. Phys. Conf. Ser.* **2017**, *917*, 062001.

Table of Content Graphic